CLOUD MICROPHYSICAL PARAMETERS FROM TOVS: A PRACTICAL SCHEME AND GEOMETRICAL CONSIDERATIONS

P.D.Watts

U.K. Meteorological Office

ABSTRACT

Inversion of cloudy TOVS radiances demands that account be taken of solar and atmospheric infrared radiation reflected from clouds.

In part 1 a simple reflection model based on two stream scattering calculations and it's application in a non-linear retrieval scheme is described. The interpretation of the retrieved reflectivity at $3.7\mu m$ (HIRS channel 19) in terms of a cloud drop effective radius is made possible by using a discrete ordinates scattering program to give the expected bidirectional reflectivity. A more direct and physically reasonable approach to modelling HIRS cloud radiative properties is described.

In part 2 AVHRR data is used to demonstrate that the effect of cloud shape on the observed reflectance is very significant. This precludes detailed inference of effective radius. However, results suggest that a large area average measurement such as that made by the HIRS instrument significantly removes the geometrically induced noise.

1. HIRS REFLECTANCE MODEL

The trend towards use and NWP assimilation of measured radiances in their raw, uncorrected, form has meant that greater attention has focussed on accurate forward modelling of the radiative transfer equation (RTE). More explicit use of the radiance data means that more explicit modelling of them is appropriate. This paper is concerned with modelling the part of the RTE concerned with clouds, particularly their spectral emissivity, reflectivity and transmission. It documents recent progress made in the UKMO in this particular modelling aspect.

Turner et al. (1991) reminded the TOVS community of the fact that clouds, even fully opaque ones, did not emit as black bodies, especially in the shortwave ($\sim 4\mu m$) band (channels 13-19). They used results of Yamamoto (1970) and Hunt (1973) to estimate opaque water cloud spectral reflectivity and showed that inclusion of reflected solar and downwelling atmospheric radiation in the RTE was important. Inclusion of such terms may have some relevance to cloud-clearing methods but is more obviously important when use is made of raw, 'cloud-contaminated' measurements.

This part of the paper summarises our attempts to formulate a model of cloud reflectivity for the HIRS instrument[1] and demonstrates the retrieval of cloud drop size information.

The major limitations of using Yamamotos' work are that it was restricted to one type of cloud and didn't cover the shortwave region beyond 5 μm. For HIRS we need information in the 4.3 μm region and on the behaviour with different cloud types. To this end, we performed Mie and two stream calculations[2] for a variety of cloud types and solar angles and examined the spectral emission and reflection functions. Examples are given in WB. We arrived at the following conclusions:

[1] Details on this section can be found in Watts and Baran (1992), hereafter WB.

[2] two stream calculations give hemispherically averaged radiative properties which depend only on solar angle, drop size distribution and optical depth, see, for example, Meador and Weaver (1980). Kirchoffs' Law applies: R+T+E=1 where R is reflectivity, T is transmittance and E is emissivity.

- For most water clouds we can assume negligible transmission and significant reflection at short wavelengths.
- The basic reflectivity pattern of peaks and troughs is fixed by the refractive index of water.
- The basic pattern appears to grow or shrink depending on the drop size (effective radius) and solar zenith angle.

This led us to a simple HIRS cloud radiative model:
The channel i reflectance is given by

$$\Re_i = \rho \Re_i^0$$

where $\Re_i^0$ is the 'basic pattern' channel i reflectance and ρ is a reflectivity parameter. We assume here that all clouds are opaque and so the emissivity is given by $\epsilon_i = 1 - \Re_i$. The values for $\Re_i^0$ are given in table 1.

Table 1. HIRS basic pattern reflectances

HIRS channel	1	2	3	4	5	6	7	8	9	10
$\Re_i^0$ %	1.7	1.6	1.5	1.5	1.5	1.3	1.3	1.0	3.0	1.1
HIRS channel	11	12	13	14	15	16	17	18	19	
$\Re_i^0$ %	3.6	2.8	3.6	3.8	4.5	5.3	9.3	11.9	13.8	

This reflectance parameterisation was incorporated into the TOVS fast forward and gradient models RTTOV, Eyre (1991). In WB we used this to establish the effect of opaque water cloud reflection on HIRS channel brightness temperatures, both the reflected solar and downwelling atmospheric radiation terms. Only the $4.3\mu m$ band channels have significant solar effects and only HIRS 18 and 19 have a large ($\sim 2K$) emission deficit.

We added the reflectance parameter to the UKMO non-linear TOVS inversion scheme, Eyre (1989a and b), and performed simultaneous retrievals of cloud fractional cover, top pressure and ρ parameter. HIRS 19 was included in the measurements used. Detailed results of this for a case study pass are given in WB but here we show only the retrieved cloud top pressure, figure 1, and the HIRS 19 % reflectivity $\Re_{3.7}$, figure 2. Correspondence between areas of high cloud-low reflectivity, medium cloud-medium reflectivity and low cloud-high reflectivity are apparant. This is consistant with the inverse drop size/ reflectance relationship[3]. It was shown in WB that the retrieved $\Re_{3.7}$ had strong angular dependence which precluded inversion of it to a drop effective radius value. The hemispherical fluxes from the two stream methods were inadequate and more detailed scattering calculations would a) enable the drop size inversion and b) provide a more reliable HIRS cloud radiative model.

1.2 Bidirectional Radiative properties

The bidirectional reflection, transmission and emission of plane parallel clouds can be obtained using the general purpose scattering program DISORT (Stamnes et al. 1988). Using 48 stream calculations for an opaque cloud, we obtained a table of $\Re_{3.7}(\theta_{sol}, \theta_{sat}, \phi_{rel}, R_e)$ for solar zenith angles, $\theta_{sol} = 0 - 90°$, satellite (view) zenith, $\theta_{sat} = 0 - 60°$, relative azimuth angles, $\phi_{rel} = 0 - 180°$ and effective radii, $R_e = 1 - 23\mu m$. This table can be interrogated for $\Re_{3.7}$ given the geometric angles and an effective radius. An inverse routine returns the drop radius given the geometry and a value of $\Re_{3.7}$. Figure 3 shows $\Re_{3.7}$ as a function of view zenith and relative azimuth for $\theta_{sol} = 50°$ and $R_e = 7\mu m$. Forward and backscattering regimes are clearly visible

[3]The high cloud is undoubtedly ice phase and not spectrally modelled appropriately by the water cloud R_i. However, by omitting channel 18 from the retrieval, we have only channel 19 with high sensitivity to solar reflection and hence the retrieved reflectivity in channel 19 is probably still accurate; the implied reflectivities in other channels could well be very wrong!

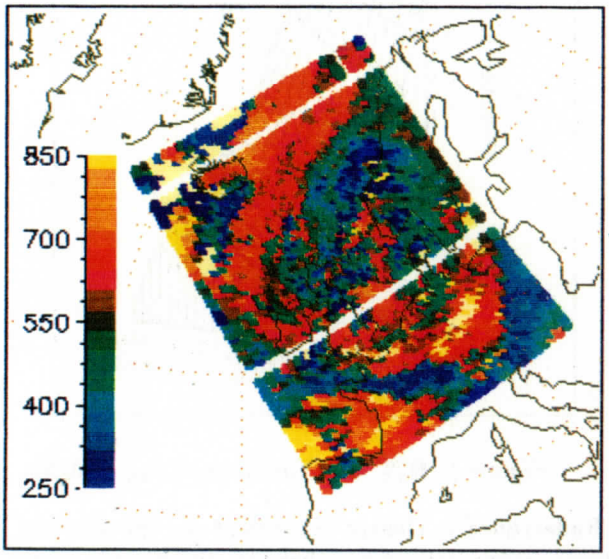

Figure 1. Retrieved cloud top pressure (mb).

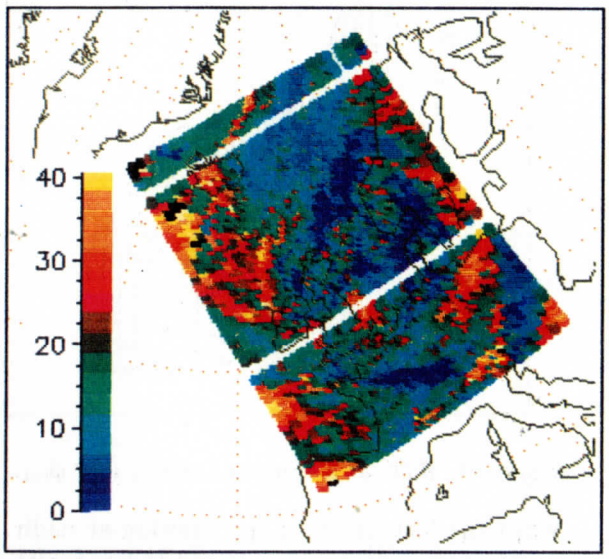

Figure 2. Retrieved $\Re_{3.7}$ (%)

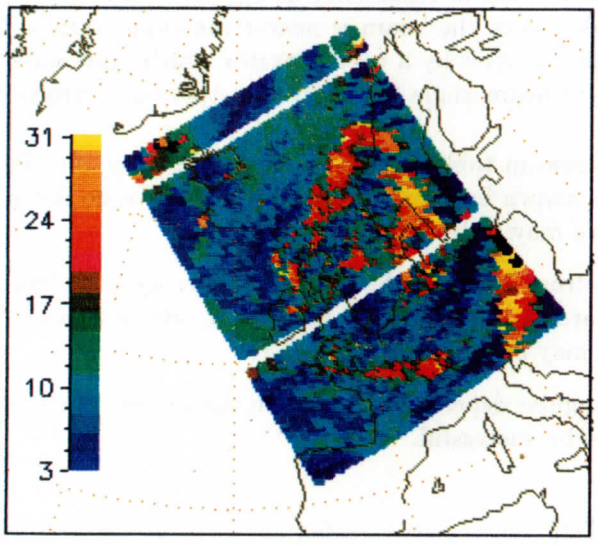

Figure 5. Retrieved R_e (μm)

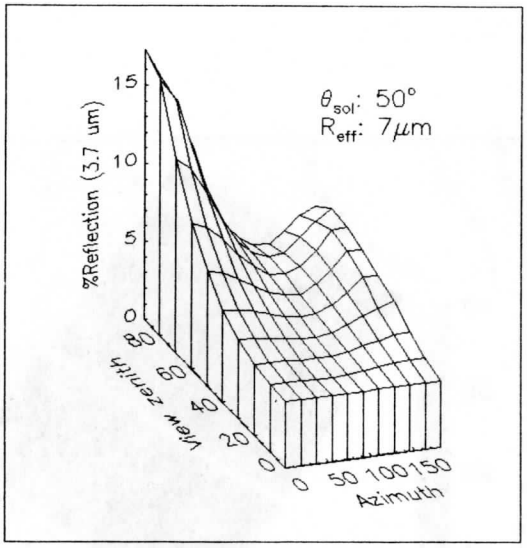

Figure 3. $\Re_{3.7}^{calc}$ as a function of θ_{sat} and ϕ_{rel}.

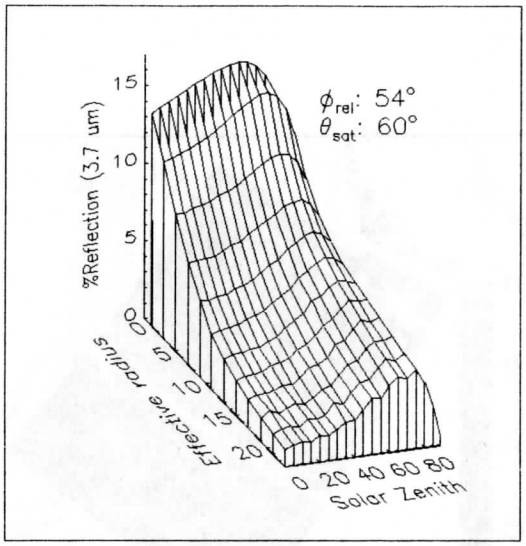

Figure 4. $\Re_{3.7}^{calc}$ as a function of θ_{sol} and R_e.

when the instrument is not viewing at nadir. Reflectance is clearly dependent on the viewing angle - more energy is scattered at low zenith angles regardless of whether the direction is more 'forward' or 'backward'.

Figure 4 shows the increase in reflectivity as θ_{sol} increases - the scattering is more efficient for more glancing angles since the beam is nearer the cloud surface for longer allowing more photons to escape. This is offset by a $\cos\theta_{sol}$ factor which represents the energy available per unit area at a particular beam angle. Clearly, also, there is a strong dependency on R_e at all solar angles.

Using the inverse look-up table we have inferred the drop effective radius from the TOVS retrieved $\Re_{3.7}$. This is shown in figure 5. Although we have no independent measurements to support these values we may at least note the following:

- R_e values range from $2\mu m$ for the small cumulus areas to $28\mu m$ for the cirrus (the reflectance tables are extrapolated for values of R_e above $23\mu m$). This is broadly in agreement with what may be expected.
- No substantial angular dependence is seen in the values - the use of the geometric look-up tables appears to be successful.

1.3 Sources of error

- Errors in the retrieved cloud parameters will cause corresponding errors in the cloud reflectivity and R_e. A simulation of this effect is possible (see, for example, Eyre 1989a). Cloud pressure error will tend to be less important since HIRS 19 is a fairly clean window and therefore not unduly affected by the height assignment. Cloud fraction is important though, and errors in it are largest for fields of view with low cloud cover. A further problem, with partially cloudy soundings is that reflection from the underlying surface becomes a factor, although (for realistic land surface reflectivities ($\leq 5\%@3.7\mu m$)) serious errors in cloud reflectivity do not occur unless the cloud fraction is as low as 20%. Clearly, retrieved R_e values will only be reliable for the cloudier soundings.
- The cloud may not be truly opaque - almost certainly true for most cirrus. We hope to address this problem by including optical depth as a further cloud parameter in the retrieval, see below.

- The base scattering calculations may be in error or unrepresentative. For example, the drop size distribution may not represent what is actually present or the real cloud may not be homogeneous in the vertical. These possibilities really question the definition of an effective radius.

- The cloud may not be truly plane parallel as assumed in the scattering calculations, i.e. it may have significant vertical structure. This question is addressed in part 2 of this paper.

- Errors in atmospheric transmittance modelling, particularly in HIRS 19, will lead to erroneous reflectivity. As part of a simultaneous retrieval of temperature and humidity the HIRS 19 transmittance is probably as well modelled as possible and, anyway, the channel is quite a good window. With a typical above cloud absorption of 0.15 and an error in this of 10% we have a transmittance error of $\sim$ 1.7%. This will give aproximately the same percentage errors in both $\Re_{3.7}$ and R_e: the effect is small.

1.4 An improved model

The two-stage process described above - retrieval of a reflectivity parameter ρ followed by the inversion of $\Re_{3.7}$ to R_e - is clumsy and does not model the HIRS spectral cloud properties to the best of our knowledge. For example, to account for transmitting clouds we would have to introduce a transmittance parameter and somehow relate it to ρ. We therefore plan to replace ρ with R_e both in RTTOV and in the non-linear inversion scheme. R_e will be connected to cloud reflectivity via the geometric look-up tables. At the same time, we will extend the look-up tables to include optical depth τ and will experiment to see if the HIRS data can discrimate between R_e and τ. It is likely that HIRS 20 will be useful here since reflectance at $0.7\mu m$ is insensitive to drop size (Arking and Childs 1985).

The reflectance properties of ice clouds are substantially different to that of water clouds; generally lower reflectance due to lower water contants and larger drop size, but also with characteristically high side scatter. There appears to be no conveniant characteriser analogous to R_e for ice clouds although size distibutions for several cirrus types have been measured and could perhaps be used in some crude classification. One important aspect of this is the need to recognise (from the data) the phase of the cloud under observation, so that the appropriate reflectance characteristics can be used.

2. GEOMETRICAL CONSIDERATIONS

In part 1 we showed that given a flat opaque cloud it was possible, with a knowledge of the sun-sensor geometry, to estimate the drop effective radius R_e from measurements of reflected solar radiation at $3.7\mu m$. Cursory examination of AVHRR imagery, however, will convince most that the majority of clouds are not flat by any reasonable definition[1] and in Part 1 we showed that the reflection properties are highly angle dependent. One effect of non-flatness in a cloud is to locally change the sun-sensor geometry and thus the reflectivity. The question we attempt to answer here is whether this precludes the estimation of R_e from $3.7\mu m$ measurements. We do this using AVHRR data to estimate the cloud shape with a resolution of 1-2 Km in the horizontal. From this the local geometry is calculated and the expected reflectivity obtained. In comparing this with the observed reflectivity we are assuming that the effect of geometry on a horizontal scale of thousands of metres and greater dominates the effect of that on smaller scales. Primary justification for this comes from realising the penetration depth of $3.7\mu m$ radiation is typically hundreds of metres so that structure on a scale less than this will tend to be unimportant. Also,

[1] The definition, however, depends on the application. For example, representation by an equivalant flat cloud is adequate, in most cases, for modelling the emitted thermal radiation (Watts, 1990).

since $\Re_{3.7}$ is relatively low ($\sim$ 10%), inter-cloud reflections should be negligible. The only real justification however, comes from the agreement between calculated and observed reflectances.

We demonstrate that for interpretation of high spatial resolution reflected 3.7 μm radiance in terms solely of a cloud drop effective radius, a flat cloud model or assumption is far from generally valid. An appreciable amount of the variance in the observed $\Re_{3.7}$ field is explained solely in terms of the broad scale (> 1 Km in the horizontal) geometry.

The question of whether the averaging characteristic of a low resolution measurement revalidates the use of a flat cloud model is addressed.

Finally, a method which estimates the local effective radius and temperature lapse rate for a group of high resolution pixels is suggested.

2.2 Local cloud geometry

The kernal of this study is representation of the physical geometry of the cloud field and it's consequent effect on the source-sensor geometry. This in turn can be used to examine the effect on the expected reflectance for a given drop effective radius. The basic assumptions of the first step are that the 11 μm measurements of AVHRR channel 4 can be interpreted as the physical temperature of the cloud (or at least, the physical temperature at a constant depth in the cloud) and that the atmospheric lapse rate is at least locally constant. Calculations show that for opaque clouds the emissivity at 11μm rarely falls below 98% even for extreme view angles. Also, the atmospheric transmittance at 11 μm is sufficiently high that differences between measured brightness temperature and physical surface temperature rarely exceed 1K. Since this difference is primarily due to water vapour, it is less still when only the atmosphere above the cloud level is of interest. Consequently we expect the measured brightness temperature at 11 μm to be a fair measure of the temperature of the cloud. In conjunction with an assumed lapse rate Γ, the temperature can be interpreted as a height. It is a relative height since we do not consider the surface temperature, but for the purpose of establishing the cloud geometry, relative height is entirely sufficient. Further, because temperature *differences* are used, errors implicit in the above assumptions (atmospheric attenuation and cloud emissivity at 11μm) tend to cancel.

The method will, of course, seriously break down at cloud edges or where the cloud is significantly transmitting. However, these areas can be identified (Saunders et al., 1986) and do not represent a serious limitation.

The second step is to calculate the local sun-sensor geometry from the gradient of the height field. The details of this are given in the Appendix.

With a suitable choice of R_r it is now possible to use the look-up tables to estimate the expected local $\Re_{3.7}$.

2.3 Observed reflectance

To check the validity of the above method we need to compare the predicted reflectivity to that observed. This latter we obtain by the following equation:

$$\Re_{3.7}^{obs} = \frac{R_{3.7} - B_{3.7}(BT_{11\mu m})\tau\epsilon_{3.7}}{\tau^2 I_{3.7}^s}$$

Where $R_{3.7}$ is the measured channel 3 radiance, $B_{3.7}(BT_{11\mu m})$ is the Planck function at 3.7μm of the 11μm brightness temperature, τ is the approximate channel 3 transmittance to space, $I_{3.7}^s$ is the TOA 3.7μm solar irradiance and $\epsilon_{3.7}$ is the geometry dependent 3.7μm emissivity. The second term in the numerator is the thermally emitted radiance. $\tau_{3.7}$ we take to be a simple function of pressure and accept there will be some small loss of accuracy in not modelling it correctly. $\epsilon_{3.7}$ is obtained from the scattering calculations and so the 'observed' $\Re_{3.7}$ actually

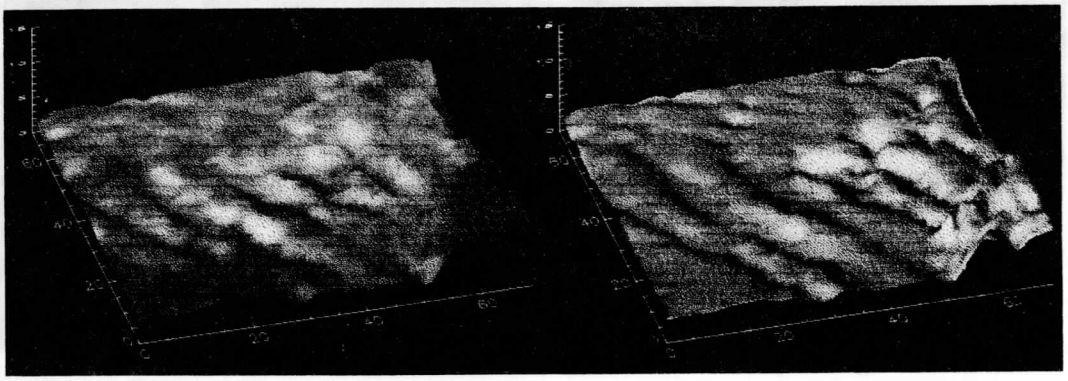

Figure 6. Wave cloud case: shading by value of $\Re_{3.7}^{obs}$ (left plot) and $\Re_{3.7}^{calc}$ (right plot)

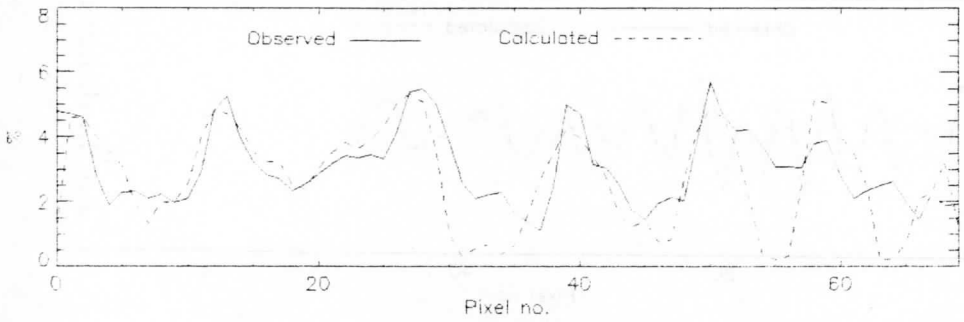

Figure 7. Wave cloud case: Cross-section of $\Re_{3.7}^{obs}$ and $\Re_{3.7}^{calc}$.

includes a small computed component[5]

2.4 Results: 2 cases

We restrict the presentation of results to two cases: one of wave clouds of considerable amplitude and horizontal scale and one of an area of stratus.

Figure 6 shows shaded isometric plots of the cloud height field for the wave cloud case; shading in the left plot represents $\Re_{3.7}^{obs}$ calculated from the above equation, shading in the right plot represents values from the look-up tables assuming $R_e = 7\mu m$. The mean ϕ_{rel} is about 185° (backscattering), θ_{sol} about 70° and θ_{sat} about 50°. The area shown is 70 × 70 pixels. The lapse rate Γ required for a reasonable fit was perhaps rather low at 4 KKm^{-1}, however, it does not necessarily represent the true atmospheric lapse rate.

All the predominant features of the observed reflectance are present to greater or lesser degree in the calculated field; significant variance, in fact, can be said to be due to geometrical effects. The area in the bottom right corner which shows as dark in the observed and light in the calculated is the edge of a band of cirrus; the R_e of $7\mu m$ is not appropriate here. Figure 7 is a cross-section of figure 6 25 pixels up from the bottom. This clearly emphasises that a large proportion of the variation in $\Re_{3.7}^{obs}$, perhaps 80%, is explained by the geometry. Also seen is that the calculated values are too low on the anti-sun (RH) side of cloud masses.

The second case is for a very flat stratus area near the AVHRR scan centre and is shown, as for the wave case, in figures 8 and 9. ϕ_{rel} is again ~ 185°, θ_{sol} ~ 60°, θ_{sat} ~ 5°, $\Gamma = 6KKm^{-1}$

[5]This is necessary to keep reflectivity as the variable of interest - we could have avoided it by comparing radiances, however, it in no way invalidates the results.

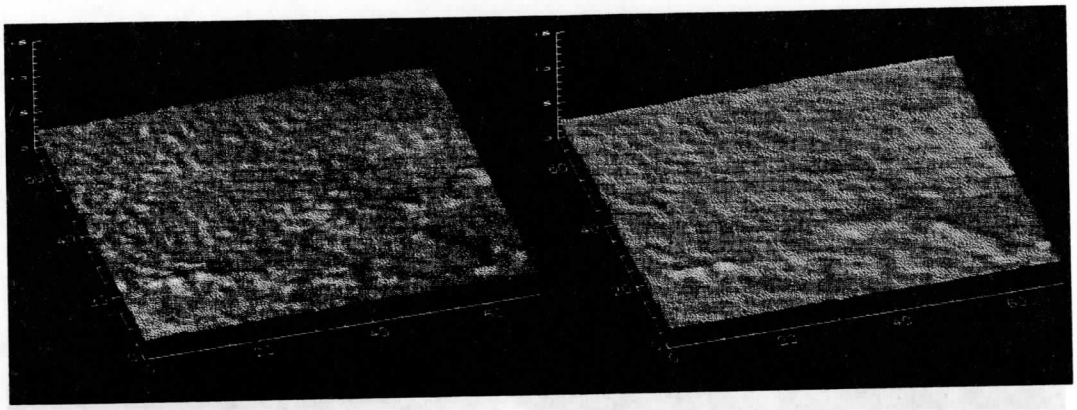

Figure 8. Stratus cloud case: shading by value of $\Re_{3.7}^{obs}$ (left plot) and $\Re_{3.7}^{calc}$ (right plot)

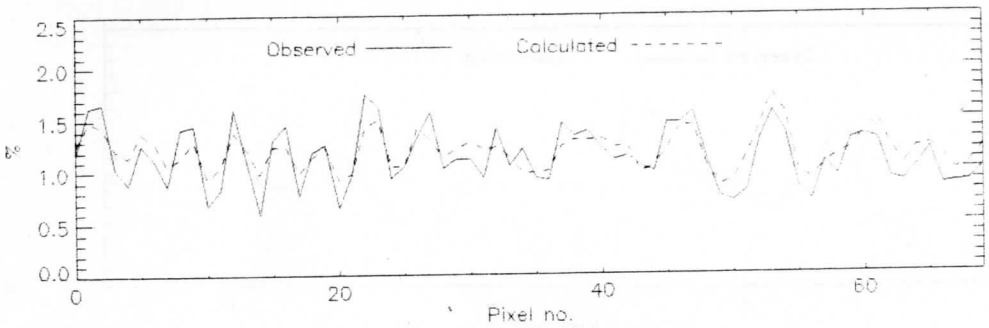

Figure 9. Stratus cloud case: Cross-section of $\Re_{3.7}^{obs}$ and $\Re_{3.7}^{calc}$.

and $R_e = 12\mu m$. Again, the calculated field has the general appearance of the observed field and the cross-section shows very good agreement with peaks and troughs in exactly the same position. The amplitude of the variation in the calculated field is significantly lower than that in the observed; this is probably due to the finite differencing for the gradient field tending to smooth the real gradient. This time, with a very flat cloud the geometrically caused variance is less - 30-40% of the total reflectance.

These two extreme cases have shown that much of the observed variance in AVHRR channel 3 reflectance from water clouds can be attributed to the geometry of the cloud top. It can hardly be said to be a comprehensive study as there is such a diversity of cloud types and situations to make this a huge task. We *can* find areas of cloud where the $\Re_{3.7}^{obs}$ appears to bear only passing resemblence to the calculated values. Sometimes this will be due to the cloud being thin, broken or of ice or mixed phase but sometimes any plausible explanation is elusive.

Further, although the general features of the reflectance pattern are reproduced the accuracy to which this is done is not sufficient to enable us to significantly remove geometrical effects from the signal. This appears, at least in part, to be due to the approximate nature of our estimation of the local gradient: rapidly changing gradients are inevitably smoothed.

2.5 Spatial averaging

Our limited success, however, does mean we can have confidence in estimating the effect of geometry on drop size retrieval. In particular, we are interested in the averaging effect of a large footprint sounder such as HIRS/2. Using the computed reflectances for the wave cloud case, we can invert a reflectance to obtain an R_e value. Of course, using the local geometry we obtain the R_e assumed in the computation. However, using the simple flat cloud geometry we get an R_e which is in error. We have done this here for a single AVHRR pixel, marked * on figure 6, and

to be constant. The suggested technique is to minimise the function:

$$F(\Gamma, R_e) = \sum_i^n (\Re_{3.7_i}^{obs} - \Re_{3.7_i}^{calc}(\Gamma, R_e))^2$$

where Γ determines the geometry to use in the look-up table through the height field. It is suspected that the two parameters can be estimated independently since R_e will tend to shift the mean calculated reflectance whilst Γ will primarily affect its variance. However, we have had little success with this so far, the minimum tends to to lie at very large drops and for very high lapse rates - i.e. a reflectance field with no variation. We suspect this is due to aliasing of the peaks and troughs such that a bland field better fits the observed varying field.

REFERENCES

Eyre J.R., 1989a and b: Inversion of cloudy TOVS radiances by non-linear optimal estimation. I:Theory and simulation for TOVS. II:Application to TOVS data. Q.J.R.Meteor.Soc. **115**, pp.1001-1037.

Eyre J.R., 1991: A fast radiative transfer model for satellite sounding systems. Technical Memorandum no.176, European Centre for Medium range Weather Forecasts, Shinfield Park, Reading, U.K.

Hunt G.E., 1973: Radiative properties of terrestrial clouds at visible and infrared thermal window wavelengths. Q.J.R.Meteor.Soc. **19**, pp346-369.

Meador W.E. and Weaver W.R., 1980: Two-stream approximations to radiative transfer in planetry atmospheres: a unified description of existing methods and a new improvement. J.Atmos.Sci. **37** pp.630-643.

Saunders R.W. 1986: An automated scheme for the removal of cloud contamination from AVHRR radiances over Western Europe. Int.J.Remote.Sensing, **7** pp.867-886.

Stamnes K., Tsay S.C., Wiscombe W. and Laszlo I. 1988: A general purpose numerically stable computer code for discrete-ordinate method radiative transfer in scattering and emitting layered media. To appear as NASA report, 1988.

Turner D.S. and Steenbergen J.D. 1991: Investigations of systematic errors in TOVS forward model calculations in cloudy conditions. In: Tech.Proc. 6th International TOVS study conference. Airlie, VA, 1-6 May 1991. Ed. W.P.Menzel. Report of CIMMS, Univ. Wisconsin, Madison.

Watts P.D. 1990: The validity of a flat cloud model for infrared sounding. Meteorological Office MET O 19 Branch Memorandum no. **102**, London road, Bracknell, Berks, U.K.

Watts P.D. and Baran A.J. 1992: Modelling reflecting and semi-transparant cloud for infrared modelling. To appear in: NATO Advanced Workshop on 'High sectral resolution infrared remote sensing for earth's weather and climate'. Paris, France, 23-26 March 1992.

Yamamoto G., Masayuki T. and Shoji A., 1970: Radiative transfer in water clouds in the infrered region. J.Atmos.Sci. **27**, pp.282-292.

APPENDIX: GEOMETRY

The geometric inputs to the discrete ordinates scattering radiative transfer package (DISORT) are the source (Sun) zenith, view (satellite) zenith and relative (Sun-satellite) azimuth angles. In order to calculate these values for a sloping cloud facet, it is conveniant to work with a set of orthonormal vectors defining the cloud plane and unit vectors defining the solar and satellite directions. The angles then result from simple vector dot products.

Unit vector components from zenith and azimuth angles (θ and ϕ respectively) are given by the following relations:

$$s_z = \cos\theta, \tag{1}$$

$$s_x = \cos(\phi)\sin\theta \tag{2}$$

and

$$s_y = \sin(\phi)\sin\theta. \tag{3}$$

The inverse of the above relations are:

$$\theta = \cos^{-1}(s_z) \tag{4}$$

$$\phi = \sin^{-1}(s_y/\sin\theta) = \cos^{-1}(s_x/\sin\theta) \tag{5}$$

A.1 Orthonormal vectors of the cloud surface

We have a cloud temperature field $T(x,y)$, where, conventionally, x is taken as the across track and y as the along track directions respectively. The (relative) height field is then $H(x,y) = T(x,y)/L$, where L is the, at least locally, constant lapse rate in KKm^{-1}. The gradients of the height field dH/dx and dH/dy can be found by differencing pixels in the appropriate directions. That is,

$$dH/dx = H_x = (H(x+1,y) - H(x-1,y))/2Ip$$

where Ip is the interpixel distance and, in the case of AVHRR is equal to $1.1/\cos(\theta_{sat})$. Similarly for H_y.

We now wish to establish a set of orthonormal vectors c_1, c_2, c_3 in the plane of the cloud as defined by H. We can somewhat arbitrarily let the first vector be that which projected onto the $x-y$ plane lies in the x direction, i.e.

$$c_1 = [1, 0, H_x]/(1+H_x)^2 \tag{6}$$

say.

A second vector, not orthogonal but also in the plane of the cloud, is c':

$$c' = [1, 0, H_y]/(1+H_y)^2 \tag{7}$$

The vector c_3, orthonormal to c_1 and c', is perpendicular to the cloud plane and is found through the relations $c_3.c_1 = c_3.c' = 0$ and $c_3.c_3 = 1$. This leads to

$$c_3 = [-H_x, -H_y, 1]/(1+H_x^2+H_y^2)^{1/2} \tag{8}$$

By similar method we can establish c_2, the vector orthonormal to c_1 and c_3 (and which therefore is in the cloud plane). Here we have, $c_2.c_3 = 0$, $c_2.c_1 = 0$ and $c_2.c_2 = 1$, and we find

$$c_2 = [-H_x, (1+H_x^2)/H_y, 1]/(1+H_x^2+(1+H_x^2)/H_y^2)^{1/2} \tag{9}$$

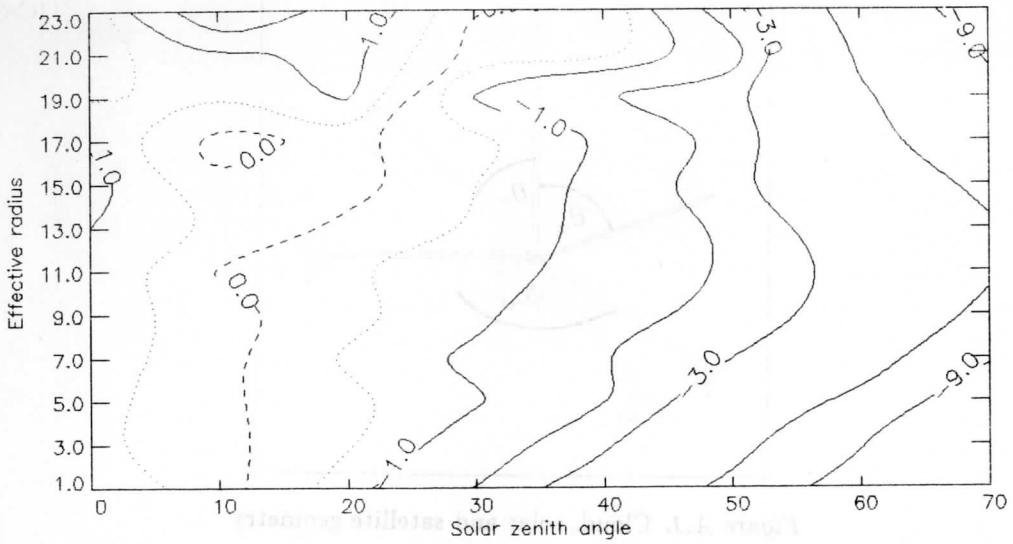

Figure 10. Example error in R_e from flat cloud assumption for 1.1 Km (AVHRR) pixel.

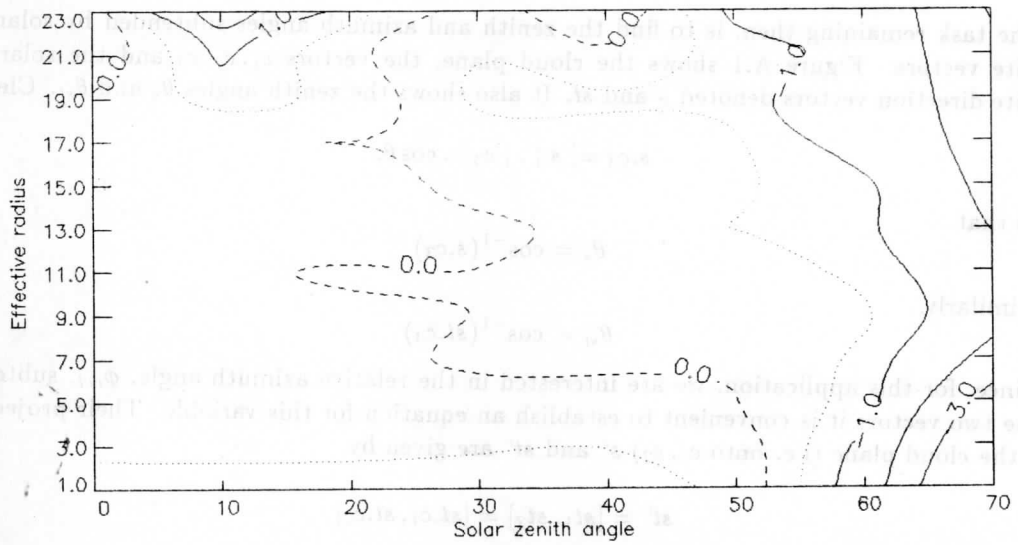

Figure 11. Example error in R_e from flat cloud assumption for 17 × 17 Km ('HIRS') pixel.

for a 17 × 17 pixel average, around the *, to represent the HIRS footprint. We have used a range of true R_e values $1 - 23\mu m$ and a range of solar zenith angles $0 - 70°$. The errors resulting are plotted in figures 10 and 11 for the 1 × 1 and 16 × 16 pixel cases respectively. They generally show the same features; larger errors result when the drop size is smaller and the solar angle is larger. This is because most rapid variation in the reflectivity function occurs in these cases (see figures 3,4). It is also clear that the effect of the area averaging of the 'HIRS' footprint is to significantly reduce the error in the flat cloud estimation of R_e and allow higher solar zenith angles to be used.

Again, these results are somewhat specific to the particular case chosen although the general conclusion is likely to remain true for any cloud. More thorough employment of the above technique could establish acceptable limits on the use of HIRS data for R_e estimation.

2.6 Combined lapse rate-drop size estimation

An intriguing possibility exists of simultaneously estimating the local lapse rate and cloud drop radius using a colloction of n AVHRR pixels close enough that the two variables are likely

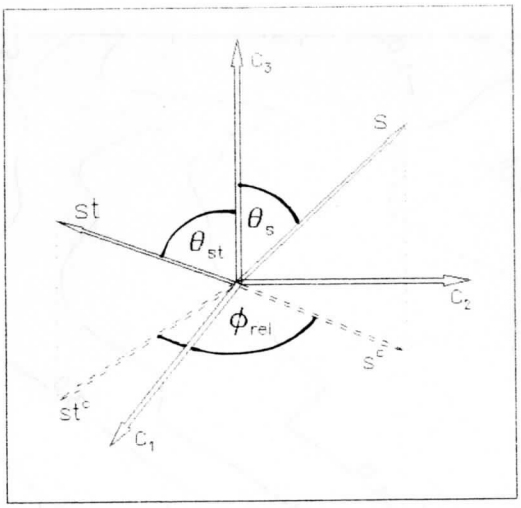

Figure A.1. Cloud, solar and satellite geometry

A.2 Angles relative to the cloud plane

The task remaining then, is to find the zenith and azimuth angles subtended by solar and satellite vectors. Figure A.1 shows the cloud plane, the vectors c_1, c_2, c_3 and the solar and satellite direction vectors denoted s and st. It also shows the zenith angles θ_s and θ_{st}. Clearly,

$$s.c_3 = \mid s \mid . \mid c_3 \mid . \cos\theta_s \tag{10}$$

so that

$$\theta_s = \cos^{-1}(s.c_3) \tag{11}$$

and similarly,

$$\theta_{st} = \cos^{-1}(st.c_3) \tag{12}$$

Since, for this application, we are interested in the relative azimuth angle, ϕ_{rel}, subtended by the two vectors it is convenient to establish an equation for this variable. Their projections onto the cloud plane (i.e. onto c_1, c_2) s^c and st^c are given by

$$st^c = [st_1, st_2] = [st.c_1, st.c_2] \tag{13}$$

$$s^c = [s_1, s_2] = [s.c_1, s.c_2] \tag{14}$$

Now,

$$st^c.s^c = \mid st^c \mid . \mid s^c \mid . \cos(\phi_{rel}) \tag{15}$$

So that the relative azimuth is given by

$$\phi_{rel} = \cos^{-1}(st_1.s_1 + st_2.s_2)/((st_2^2 + st_1^2)^{1/2}.(s_2^2 + s_1^2)^{1/2}) \tag{16}$$

TECHNICAL PROCEEDINGS OF

THE SEVENTH INTERNATIONAL TOVS STUDY CONFERENCE

Igls, Austria

10-16 February 1993

Edited by

J R Eyre

European Centre for Medium-range Weather Forecasts
Shinfield Park, Reading, RG2 9AX, U.K.

July 1993